

Structural and optical characterization of synthetic diamonds in nano, micro and millimetre scale

© A. Olejniczak¹, R. Tomala^{1,¶}, P. Žemojtel¹, A.F. de Araujo Maia^{1,2}, O. Bezkravnyj¹, B. Macalik¹, O. Ignatenko³, D. Beben^{1,2}, W. Stręk¹

¹ Institute of Low Temperature and Structure Research Polish Academy of Sciences, 50-422 Wrocław, Poland

² Nanores Sp. Z o. o. Sp. K., 51-317 Wrocław, Poland

³ Scientific and Practical Materials Research Center, National Academy of Sciences of Belarus, 220072 Minsk, Belarus

¶ e-mail: r.tomala@intibs.pl

Received July 15, 2021

Revised September 24, 2021

Accepted September 27, 2021

Synthetic diamonds are the subject of research in many different implementations. Recognition of the properties of materials with dimensions near the nanometre scale is of great importance for essential science and multiple applications. Microdiamonds synthesised by the HPHT method and nanodiamonds made by detonation were evaluated using XRD, SEM, TEM and Raman spectroscopy. UV-VIS luminescence measurements were performed and compared with each other to assess the surface defects and grain size influence on their optical properties.

Keywords: diamonds, spectroscopy, defects.

DOI: 10.21883/EOS.2022.01.53004.39-21

Introduction

Natural diamonds are mainly between 1–3.3 billion years old and were formed at depths of 150–200 km in the upper lithospheric mantle at temperatures of 1000–1300°C and pressures of 40–60 kbar [1]. Diamonds can be also found in the places of meteorites impact [2]. For centuries diamonds were considered high-priced materials for jewellery, and the rarest examples have served as a symbol of power and nobility [3]. This situation changed in the 20th century when methods of synthetic diamonds production have been developed. The first method of synthetic diamond production was the high-pressure, high temperature (HPHT) synthesis [4]. A high purity carbon source (graphite) is heated to 1500°C at a pressure of 5 GPa. Molten metals (Fe, Ni, Co) are used to dissolve graphite and, as catalyst, reduce the temperature and pressure needed to form diamond from graphite. In the second method, namely chemical vapour deposition (CVD), diamonds are grown onto substrates from a hydrocarbon, mainly methane, and hydrogen gas mixture [5]. CVD method requires lower temperatures (700–1300°C) and pressures (less than 1 atmosphere). The last method uses explosions to convert carbon substrate into diamond nanocrystals, so-called detonation nanodiamonds [6,7]. The development of synthetic diamond production has allowed using diamonds commercially for cutting, polishing, optics, electronics or as synthetic gemstones for jewellery [8–10]. Diamond as wide-bandgap material can be considered as a matrix for optically active ions and colour centres [11–13]. Micrometer-sized diamond powders were recently investigated as a promising material for white-lighting applications [14]. However, synthetically produced diamonds are not free from defects,

like dopants or sp²-hybridized structural changes [15]. Common nitrogen-related impurities can form multiple colour centres and reduce the transparency of synthesized diamonds [16,17]. The purpose of this work is to investigate synthetic diamonds of various sizes from nano- to millimetre scale. Structural properties are examined in terms of XRD and Raman measurements as well as electron microscopy imaging. Then the optical properties are investigated to check the influence of various sizes of diamond grains on their potential spectroscopic applications.

Experimental

Micro-diamond powder (100 μm) and diamond plate (2 mm) were synthesized using HPHT sintering technique. An alloy of nickel and manganese was used as a catalyst. Graphite powder, together with the catalyst, was stirred for 20 h. Then, the reaction mixture was compressed at 0.2 GPa in a cylinder-shaped form with 12 mm in diameter and 10 mm in height. Nanodiamond powder was synthesized by detonation from a solid mixture of different kinds of materials consisting of carbon such as micro graphite, carbon black, and ultra-dispersed diamond. A mixture of 40% of TNT and 60% of hexogen was used as an oxidation reagent. Synthetic diamond powders with grains sizes about 500 nm and 1–2 μm were bought from EID Industrial Diamonds company (catalogue numbers ERD-UM 0–0.50 and ERD-UM 1–2 respectively). Powder X-ray measurements were done using a PANalytical X'Pert Pro diffractometer (Cu Kα1: 1.54060 Å). Raman measurements were performed using Renishaw InVia Raman microscope equipped with a confocal DM 2500 Leica optical microscope and a

CCD detector in back-scattering geometry. The Raman spectra were recorded under excitation with an argon laser emitting at a 514 nm and 20x LWD objective in a single scan with a 20 s exposure time in the spectral range 100–3300 cm^{-1} . The position of the Raman peaks was calibrated before data collection using a Silicon reference sample as an internal standard with the peak position at 520.3 cm^{-1} . Powder samples had their morphology characterized through electron microscopy with the Helios G4 PFIB CXe DualBeam FIB/SEM operating at 2 kV and 0.2 nA. The diamond plate with had its topography characterized through atomic force microscopy using the NanoSurf FlexAFM in contact mode. Transmission Electron Microscopy (TEM) measurements were made with a Philips CM-20 SuperTwin TEM microscope, operating at 160 kV. Absorption spectra were measured using Agilent Cary 5000 UV-VIS-NIR spectrophotometer equipped with a Praying Mantis attachment from Harrick to measure in the reflection mode. The Al_2O_3 powder with a average grain sizes of 50 nm was used as the reference. The emission spectra were measured with Stellarnet Silver-Nova Spectrometer and CNI Lasers 266 nm 50 mW laser diode as an excitation source. Luminescence decays were measured using a Libra laser from Coherent (1 mJ, 89 fs), an OPerA-Solo Optical Parametric Amplifier and a Streak Camera from Hamamatsu.

Results and discussion

Five diamond samples were investigated, including four powder samples with average grain sizes of 5 nm, 500 nm, 1–2 μm and 100 μm and one diamond plate square with a side of 2 mm. The structure of powder samples was investigated within XRD measurements (Fig. 1). The nanodiamonds (5 nm) sample shows a broad signal at about 17° that originates from the amorphous carbon phase [18] and a slope at about 26° being a signal from the graphite phase. One may see that the broad peak assigned to the amorphous phase is about five times more intense than the first (111) diamond reflection, indicating a high contribution of the amorphous carbon phase into the final nanodiamond's structure. The remaining powder samples show good crystallinity and no presence of other phases. The morphology of the synthetic diamonds was later investigated within electron microscopy methods (Fig. 2). The largest microdiamonds (100 μm) are characterized by the excellent crystallinity of individual grains. One may distinguish a large number of grains with symmetrical shapes, i.e. octahedrons, truncated octahedrons or cuboctahedrons. However, more distorted, twinned, and defective grains are also present. With a decrease in average size, individual grains become more irregular. Only a small number of individual grains with high symmetry shapes are present for 1–2 μm and 500 nm samples. For the 1–2 μm sample, there are some grains with flat surfaces similar to the 100 μm sample; however, irregularities and surface damages play a more

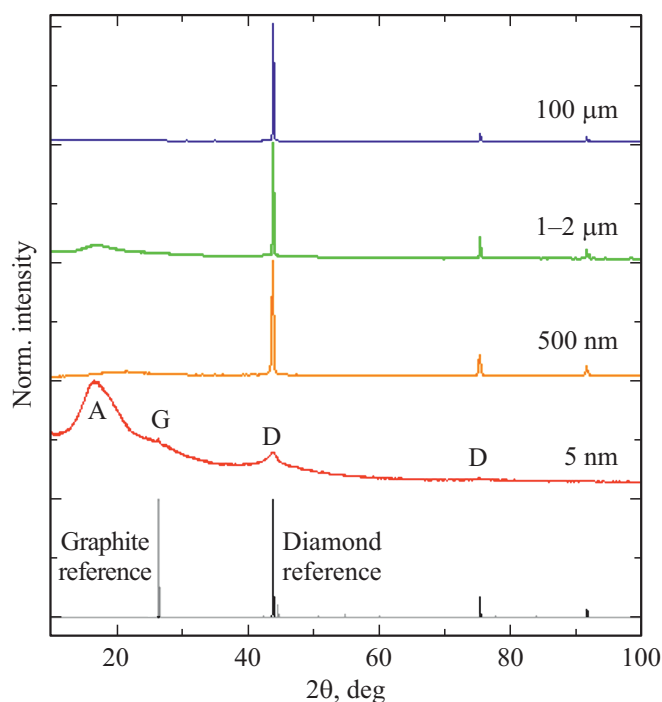


Figure 1. Powder diffraction patterns for the studied diamond samples of various sizes. For a nanodiamond sample reflections from the diamond (D), graphite (G), and amorphous (A) phases are shown.

critical role in the overall morphology of individual grains. Since the size of detonation nanodiamonds was too small for SEM imaging, its morphology was investigated using the TEM method (Fig. 3). Grains are characterized by a spherical-like shape with high tendency to agglomeration. Moreover, with decreasing average grains size, the samples show an increased tendency to agglomerate due to their increased surface energy. The crystallinity of the sample was further confirmed within electron diffraction (Fig. 3, c). An initial SEM imaging of a diamond plate surface has shown the occurrence of densely arranged square-like defects (Fig. 4, a). More precise characterization of the plate's surface using AFM has shown that the square-like defects are about 100 nm in size and 20–40 nm deep (Fig. 4, b). Such defects can serve as an active centre for the graphitization process upon heating [19] or intense laser excitation [20]. Raman spectroscopy was utilized to examine further the surface of the samples (Fig. 5). A band at 1332 cm^{-1} characteristic for sp^3 -hybridized diamond structure [21] was observed for all investigated samples. The ratio of diamond band intensity to the background increases with increasing of the sample grains size. However, the diamond band is barely seen in the detonation nanodiamond sample due to the significant contribution of amorphous carbon surrounding sp^3 -hybridized cores of individual nanodiamonds grains. It stands in The diamond plate shows the highest crystallinity among all samples. It is the only sample for which second-order Raman bands of a diamond

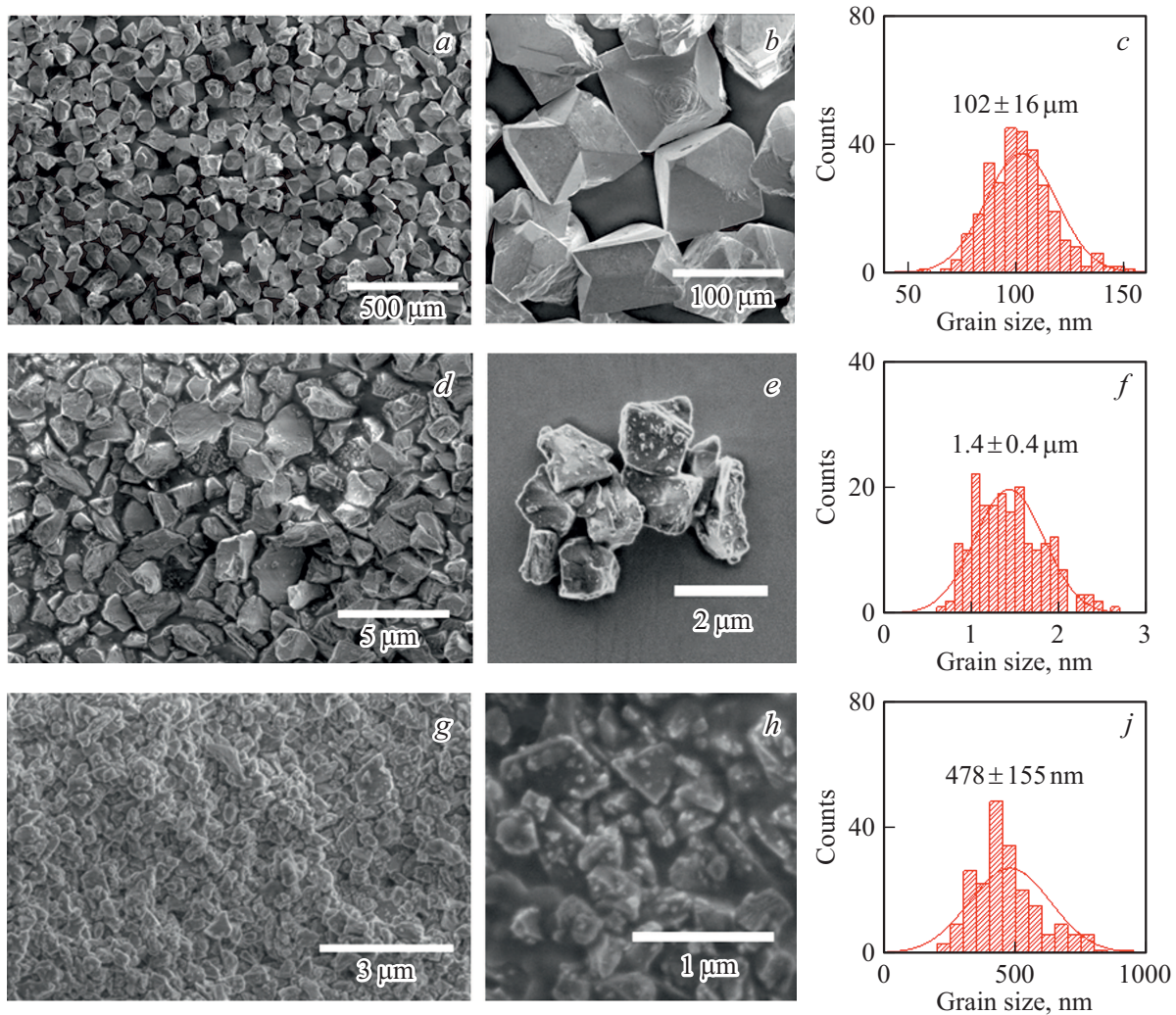


Figure 2. Representative SEM images (*a, d, g*), close-ups (*b, e, h*) and histograms (*c, f, i*) of powdered diamond samples. Microdiamonds of size $100\ \mu\text{m}$ (*a–c*), microdiamonds of size $1–2\ \mu\text{m}$ (*d–f*) and nanodiamonds of size $500\ \text{nm}$ (*g–i*).

structure are visible at $2458\ \text{cm}^{-1}$, and $2667\ \text{cm}^{-1}$ [21]. The remaining powder samples show broadband centered at about $2100\ \text{cm}^{-1}$ which can be associated with nitrogen impurities forming NV^0 centres [22]. The microdiamonds powder sample ($100\ \mu\text{m}$) shows an additional band centered at about $865\ \text{cm}^{-1}$, possibly originating from nickel related defects [23,24] from the nickel-manganese catalyst used in the HPHT synthesis process. One may see that no bands characteristic for sp^2 -hybridized graphite structure [25] (i.e. D band at $1350\ \text{cm}^{-1}$, G band at $1582\ \text{cm}^{-1}$, G' band at $2700\ \text{cm}^{-1}$) were observed. Although surface defects were clearly visible in all samples within SEM/AFM imaging, no surface reconstruction to graphite structure was detected. Such an outcome can result from surface sp^2 -hybridized atoms not forming a typical arrangement, and their response in the Raman scattering process is overshadowed by the strong Raman response of the sp^3 -hybridized matrix. It was observed that the colour of the investigated diamond samples depends on grain size and the

method of synthesis. The colour changes from dark-grey for the $5\ \text{nm}$ sample, through white for $500\ \text{nm}$ and $1–2\ \mu\text{m}$ samples and green for the $100\ \mu\text{m}$ sample to yellow for the diamond plate. It is confirmed by diffuse-reflectance measurement of samples collected at room temperature (Fig. 6). The grey colour of the $5\ \text{nm}$ sample comes from mixing crystalline nanodiamonds with amorphous carbon, which is black. There are no intense bands beyond the absorption edge in samples for $500\ \text{nm}$ and $1–2\ \mu\text{m}$, which is confirmed by their white colour. In contrast to smaller samples, the microdiamonds and the diamond plate demonstrate broadband covering the UV and blue spectrum. It is typical for Ib-type of diamonds [26]. As reported, the colour centres in diamonds are related to defects in their structure [15,26]. In samples synthesized by the HPHT method, the defect associated with the occurrence of nitrogen atoms was dominating [27]. The type of C-defects, A-defects, B-defects and N3-defects related with aggregation of single nitrogen atoms into different type complexes are

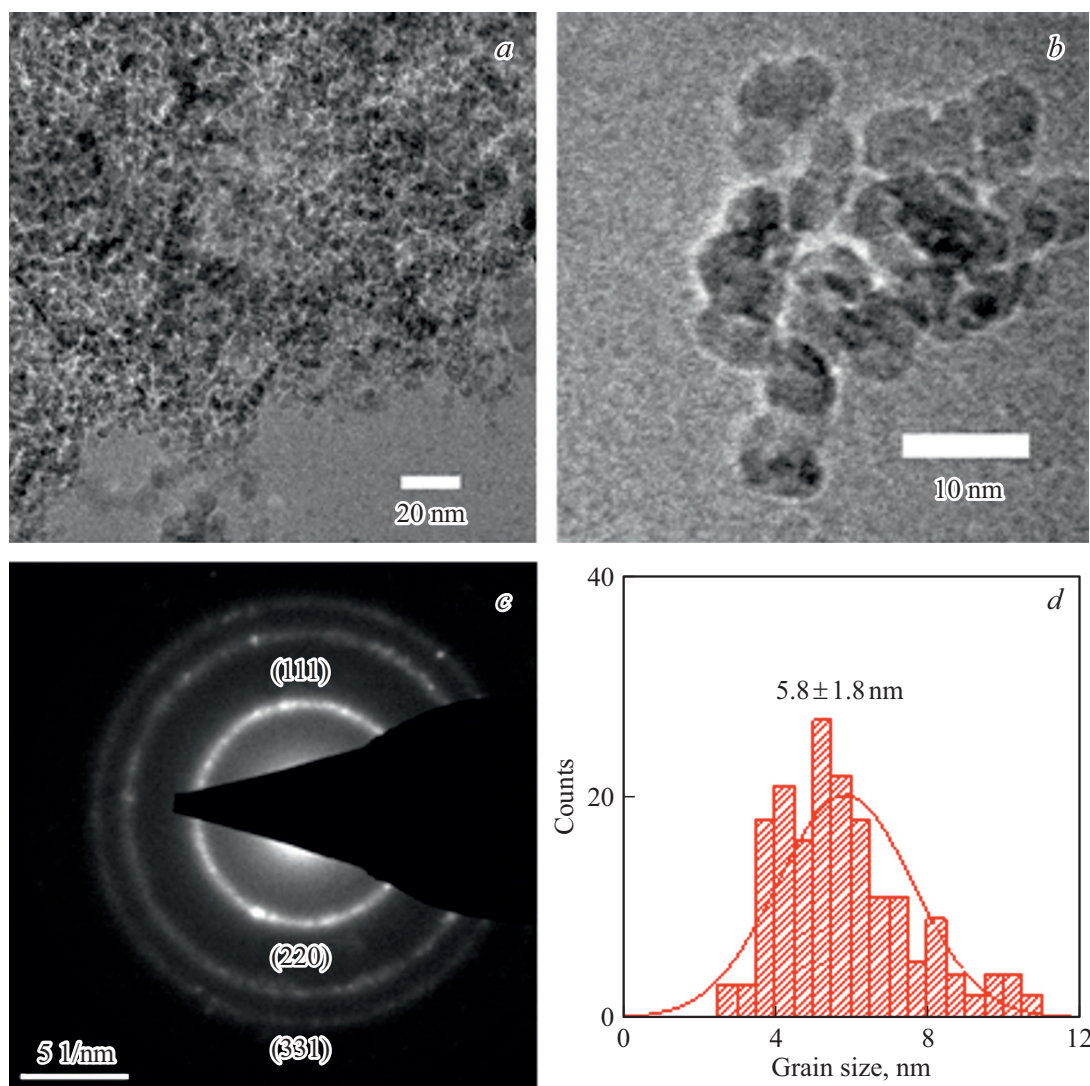


Figure 3. Typical TEM image (a) and close-up (b) of the detonation nanodiamonds sample. Diamond structure confirmed by electron diffraction (c). Histogram of nanodiamond grain sizes (d).

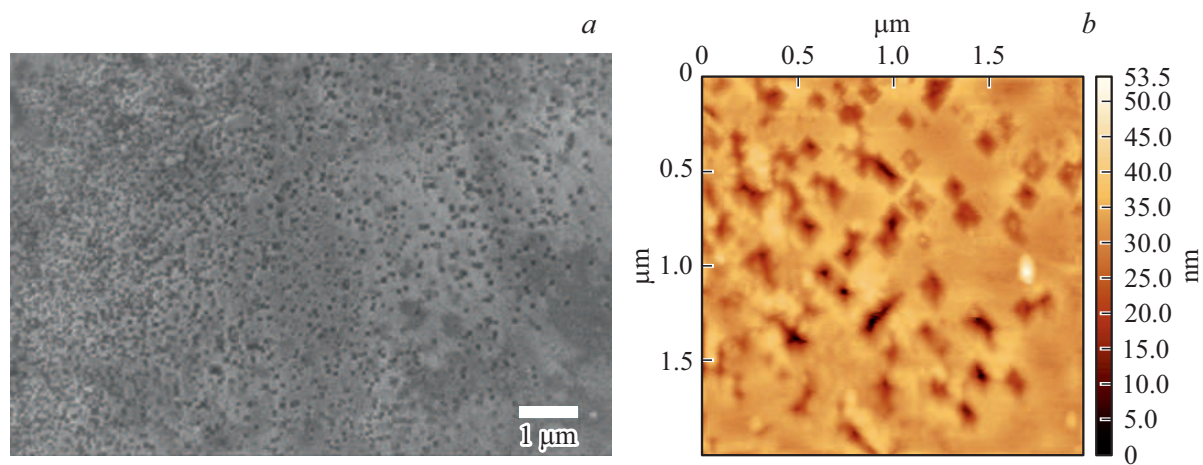


Figure 4. Typical images of HPHT diamond plate using SEM (a) and AFM (b).

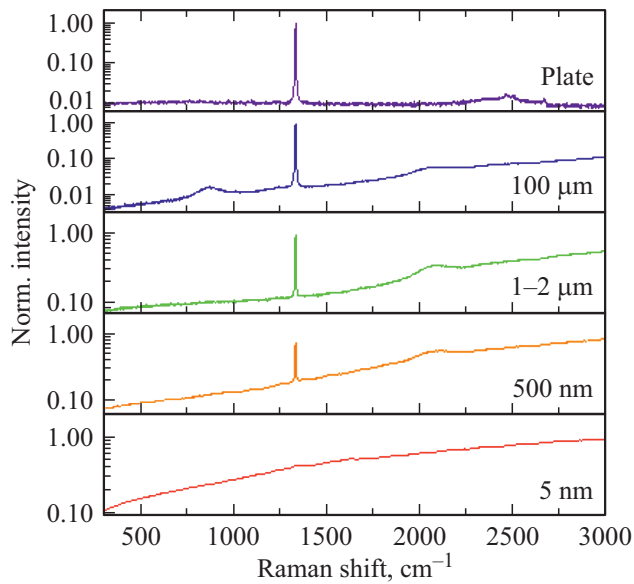


Figure 5. Raman scattering spectra of the studied diamond samples of different sizes.

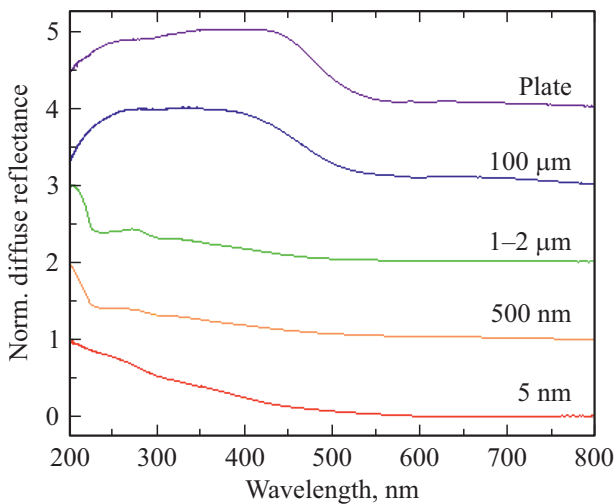


Figure 6. Diffuse reflectance spectra of the studied diamond samples in the visible and near UV ranges.

present in the samples. Under the excitation of 266 nm laser at room temperature, the samples besides the 5 nm exhibit broadband luminescence in the UV-VIS range (Fig. 7). The lack of luminescence by the 5 nm sample is most likely related to photons' self-absorption by amorphous carbon present in the sample. It was observed that the emission band for each sample consists of several overlapping bands. The room temperature measurements preclude to precise determination of position and intensity of each compound. The emission band of the 500 nm sample is centred at 450 nm, and the emission of 1–2 and 100 μm is centred at 531 nm. Moreover, the emission of the diamond plate is centred at 498 nm. As shown, the formation of defects is dependent on the annealing temperature during the

synthesis process [28,29]. The decay time of luminescence has been presented on Fig. 8. The decay has been measured at room temperature and registered at maximum of emission band. It was observed that the luminescence exhibit non-single exponential behaviour what is related to emission from different type of defects. Generally the tendency that decay time decreased with the size of diamond is observed, but phenomena is strongly related to the type of defects in diamond structure.

Conclusions

This work provides an analysis of synthetic diamonds, assessing luminescence spectra based on the different grain sizes. The present findings confirm a strong effect connected

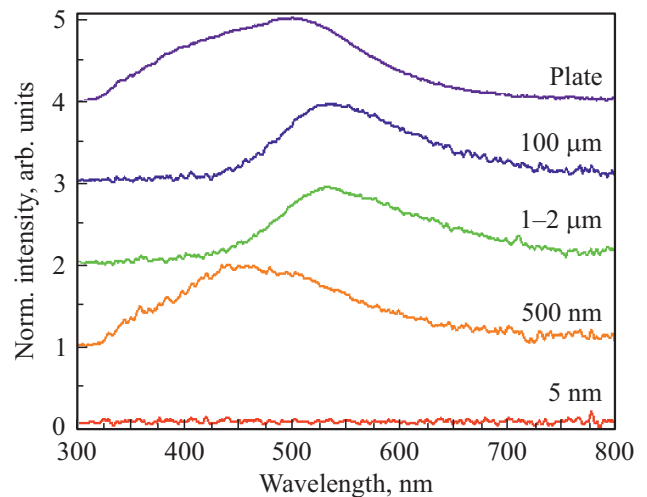


Figure 7. Luminescence spectra of the studied samples upon excitation by diode laser with wavelength of 266 nm.

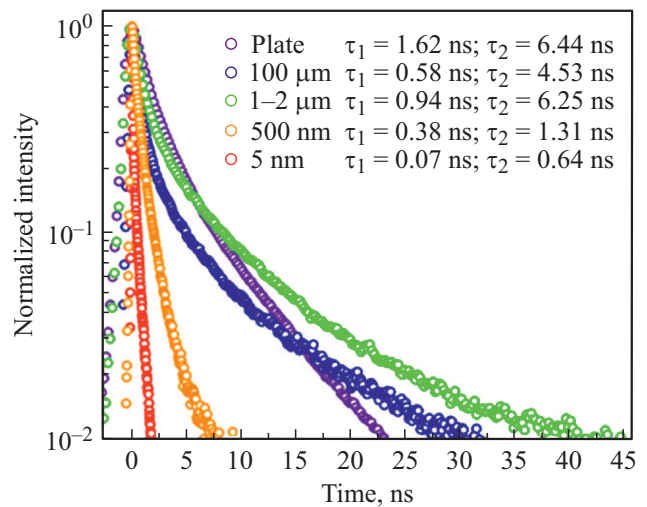


Figure 8. Luminescence decay curves of the studied diamond samples upon excitation at wavelength of 266 nm, recorded at the maximum of the emission bands (for the sample of 5 nm at 450 nm).

to the samples. diameter. Colour varies in each case, from green, which would come from residual material after synthesis, through white, down to grey. an outcome of the defects on the surface. The crystallinity of the samples was decreasing together with the size of the specimen. On the smaller diamonds, the contribution of the amorphous and sp²-hybridized carbon near the surface was of paramount importance. The Raman spectra were influenced by the structure and morphology of the particles, so the diamond bands were barely visible. This impact was also apparent in the luminescence measurement, as the lowest size sample had the least evident luminescence spectra. Overall, the results demonstrate an impact of the grain diameter and the synthesis method on the surface atoms arrangement and properties.

Acknowledgments

This work was financed by the National Science Centre Poland within the OPUS 15 (2018/29/B/ST5/00819) grant. The authors thank Ewa Bukowska for the XRD measurement.

Conflict of interest

The authors declare that they have no conflict of interest.

References

- [1] G.P. Bulanova. *J. Geochemical Explor.* **53**, 1 (1995).
- [2] F. Nestola, C.A. Goodrich, M. Morana, A. Barbaro, R.S. Jakubek, O. Christ, F.E. Brenker, M.C. Domeneghetti, M.C. Dalconi, M. Alvaro, A.M. Fioretti, K.D. Litasov, M.D. Fries, M. Leoni, N.P.M. Casati, P. Jenniskens, M.H. Shaddad. *Proc. Natl. Acad. Sci. U.S.A.* **117**, 25310 (2020).
- [3] D.C. Kinsey. *J. Br. Stud.* **48**, 391 (2009).
- [4] H.T. Hall. *Rev. Sci. Instrum.* **31**, 125 (1960).
- [5] M. Schwander, K. Partes. *Diam. Relat. Mater.* **20**, 1287 (2011).
- [6] P.S. Decarli, J.C. Jamieson. *Science* (80-.). **133**, 1821 (1961).
- [7] V.Y. Dolmatov. *Russ. J. Appl. Chem.* **79**, 1913 (2006).
- [8] V.N. Mochalin, O. Shenderova, D. Ho, Y. Gogotsi. *Nat. Nanotechnol.* **7**, 11 (2011).
- [9] N. Nunn, M. Torelli, G. McGuire, O. Shenderova. *Curr. Opin. Solid State Mater. Sci.* **21**, 1 (2017).
- [10] M.D. Torelli, N.A. Nunn, O.A. Shenderova. *Small* **15**, 1902151 (2019).
- [11] K.N. Boldyrev, B.N. Mavrin, P.S. Sherin, M.N. Popova. *J. Lumin.* **193**, 119 (2018).
- [12] B.Z. Malkin, N.M. Abishev, E.I. Baibekov, D.S. Pytalev, K.N. Boldyrev, M.N. Popova, M. Bettinelli. *Phys. Rev. B* **96**, 1 (2017).
- [13] E.A. Ekimov, S.G. Lyapin, K.N. Boldyrev, M.V. Kondrin, R. Khmel'nikitskiy, V.A. Gavva, T.V. Kotereva, M.N. Popova. *JETP Lett.* **102**, 701 (2015).
- [14] W. Streck, A. Olejniczak, R. Tomala, B. Cichy, A. Zhaludkevich, A. Konovalova, O. Ignatenko. *Proc. SPIE* **10683**, 1068307 (2018).
- [15] J. Lindblom, J. Hölsö, H. Papunen, H. Häkkinen. *Am. Mineral.* **90**, 428 (2005).
- [16] T. Hainschwang. *Gemstone Analysis by Spectroscopy*, 3rd ed. (Elsevier Ltd., 2016).
- [17] A.M. Zaitsev. *Optical Properties of Diamond* (Springer, Berlin, 2001).
- [18] K. Iakoubovskii, M.V. Baidakova, B.H. Wouters, A. Stesmans, G.J. Adriaenssens, A.Y. Vul', P.J. Grobet. *Diam. Relat. Mater.* **9**, 861 (2000).
- [19] R.A. Khmel'nikitskiy, A.A. Gippius. *Phase Transitions* **87**, 175 (2014).
- [20] A. Olejniczak, R. Tomala, B. Cichy, P. Głuchowski, M. Jakimów, A. Zięba, L. Kępiński, O. Ignatenko, W. Stręk. *Carbon N. Y.* **146**, 438 (2019).
- [21] S.A. Solin, A.K. Ramdas. *Phys. Rev. B* **1**, 1687 (1970).
- [22] G.J. Smith, J. Ellis, R. Moussaoui, C. Pardanaud, C. Martin, J. Achard, R. Issaoui, T. Gans, J.P. Dedrick, G. Cartry. *J. Phys. D. Appl. Phys.* **53**, (2020).
- [23] A.A. Khomich, R.A. Khmel'nikitskiy, A.V. Khomich. *Nanomaterials* **10**, 1 (2020).
- [24] O.N. Poklonskaya, A.A. Khomich. *J. Appl. Spectrosc.* **80**, 715 (2013).
- [25] M.A. Pimenta, G. Dresselhaus, M.S. Dresselhaus, L.G. Cançado, A. Jorio, R. Saito. *Phys. Chem. Chem. Phys.* **9**, 1276 (2007).
- [26] N.M. Kazuchits, M.S. Rusetzky, V.N. Kazuchits, A.M. Zaitsev. *Diam. Relat. Mater.* **64**, 202 (2016).
- [27] N. Chen, H. Ma, B. Yan, L. Chen, L. Chen, L. Guo, X. Miao, C. Fang, X. Jia. *Cryst. Growth Des.* **18**, 3870 (2018).
- [28] I.N. Kupriyanov, Y.N. Palyanov, A.A. Kalinin, V.S. Shatsky. *Crystals* **10**, 1 (2020).
- [29] A.M. Wassell, C.D. Mc Guinness, C. Hodges, P.M.P. Lanigan, D. Fisher, P.M. Martineau, M.E. Newton, S.A. Lynch. *Phys. Status Solidi Appl. Mater. Sci.* **215**, 1 (2018).